HHS Public Access

Author manuscript

Med Biol Eng Comput. Author manuscript; available in PMC 2016 March 06.

Published in final edited form as:

Med Biol Eng Comput. 2016 January ; 54(1): 103–111. doi:10.1007/s11517-015-1318-3.

Determination of the unmetabolized ^{18}F-FDG fraction by using an extension of simplified kinetic analysis method: clinical evaluation in paragangliomas

Dominique Barbolosi[1], **Sebastien Hapdey**[2], **Stephanie Battini**[1], **Christian Faivre**[1], **Julien Mancini**[3], **Karel Pacak**[4], **Bardia Farman-Ara**[5], and **David Taïeb**[5]

[1]Department of Pharmacokinetics, UMR INSERM 911 CRO2, Faculty of Medicine-Pharmacy, Aix-Marseille University, 27, Boulevard Jean Moulin, 13385 Marseille Cedex 5, France

[2]Department of Nuclear Medicine, Centre Henri Becquerel and Rouen University Hospital, & QuantIF-LITIS, EA 4108, Rouen University, 1 rue d'Amiens, 76038 Rouen Cedex, France

[3]Economics & Social Health and Medical Information Processing (SESSTIM, UMR912) Aix-Marseille University, Inserm, IRD, Marseille, F-13273 France; APHM, La Timone University Hospital, Public Health Department, 264 rue Saint-Pierre 13385 Marseille Cedex 5, France

[4]Program in Reproductive and Adult Endocrinology, *Eunice Kennedy Shriver* NICHD, NIH, Building 10, CRC, Room 1E-3140, 10 Center Drive MSC-1109, Bethesda, Maryland 20892-1109 USA

[5]Department of Nuclear Medicine, La Timone University Hospital, CERIMED, Aix-Marseille University, 264 rue Saint-Pierre 13385 Marseille Cedex 5, France

Summary

Tumours with high ^{18}F-FDG uptake values on static late PET images do not always exhibit high proliferation indices. These discrepancies might be related to high proportion of unmetabolised ^{18}F-FDG components in the tissues. We propose a method that enables to calculate different ^{18}F-FDG kinetic parameters based on a new mathematical approach that integrates a measurement error model. Six patients with diagnosed non-metastatic paragangliomas (PGLs) and six control patients with different types of lesions were investigated in this pilot study using ^{18}F-FDG PET/CT. In all cases, a whole-body acquisition was followed by four static acquisitions centred over the target lesions, associated with venous blood samplings. We used an extension of the Hunter's method to calculate the net influx rate constant (K_H). The exact net influx rate constant and vascular volume fraction (K_i and V respectively) were subsequently obtained by the method of least squares. Next, we calculated the mean percentages of metabolised (*PM*) and unmetabolised (*PUM*) ^{18}F-FDG components, and the times required to reach 80% of the amount of metabolised ^{18}F-FDG (T80%). A test-retest evaluation indicated that the repeatability of our

All correspondence to: David Taïeb, Department of Nuclear Medicine, La Timone University Hospital, Aix-Marseille University, European Center of Research in Medical Imaging (CERIMED), Marseille, France: +33-4-91-38-55-58, Fax: +33-4-91-38-47-69, david.taieb@ap-hm.fr.

Disclosure statement

We report no conflicts of interest relevant to this study.

The language of this manuscript was edited by the Elsevier Editing Service.

approach was accurate; the coefficients of variation were below 2% regardless of the kinetic parameters considered. We observed that the PGLs were characterised by high dispersions of the maximum standardized uptake value *SUVmax* (9.7 ± 11, coefficient of variation CV=114%), K_i (0.0137 ±0.0119, CV=87%), and *V* (0.292 ± 0.306, CV=105%) values. The PGLs were associated with higher *PUM* (p=0.02) and *T*80% (p=0.02) values and lower k_3 (p=0.02) values compared to the malignant lesions despite the similar SUVmax values (p=0.55). The estimations of these new kinetic parameters are more accurate than *SUVmax* or K_i for *in vivo* metabolic assessment of PGLs at the molecular level.

Keywords

paraganglioma; radionuclide imaging; positron emission tomography; mathematical modelling

Introduction

PET imaging using ^{18}F-FDG is useful for grading tumours and assessing therapy or disease progression [8, 18]. The uptake of ^{18}F-FDG is often characterised by calculating the standardised uptake value (SUV) from late static imaging (typically 60±10 min after injection). However, the SUV is subject to large variability, which compromises its use for inter- and intrapatient comparisons [9, 12]. Several normalisation schemes have been proposed to reduce its variability, but they do not account for the differences in ^{18}F-FDG pharmacokinetics between individual patients. More importantly, these methods do not differentiate metabolised and unmetabolised ^{18}F-FDG components within tumour regions [8]. Kinetic parameters can differentiate tumours with limited aggressiveness from benign lesions (e.g., low-grade liposarcomas vs lipomas) [6] or help to explain discordances such as high ^{18}F-FDG uptake values in tumours with low proliferation indices.

The SUV assumes that the unmetabolised component of a radiopharmaceutical (e.g., in the blood within a tumour, in the intercellular spaces, and within the tumour cells themselves) is negligible; however, some authors have reported unmetabolised ^{18}F-FDG components as high as 67% [9]. The Patlak analysis enables the calculation of unmetabolised ^{18}F-FDG, but this method has practical constraints (e.g., the acquisition of dynamic images and continuous arterial blood sampling) [16]. Simplified methods have been proposed as alternatives to the Patlak analysis to overcome the shortcomings of SUV (i.e., Simplified Kinetic analysis - SKA, Simplified Kinetic Method -SKM), but these methods also suffer from their own limitations [11, 19]. SKA (i.e., Hunter's method) neglects the unmetabolised fraction of ^{18}F-FDG. SKM (i.e., Sundaram's method) accounts for the unmetabolised ^{18}F-FDG but is based on a rough estimation of the arterial input function. More recently, Hapdey *et al*. extended the SKA method (ESKA) and significantly improved the accuracy and precision of K_i estimates [10].

In the present study, we have calculated different ^{18}F-FDG fractions and kinetic parameters based on a new mathematical approach that integrates a measurement error model. This approach was designed for routine use and is more elaborated than SKA but less time-consuming than the Patlak graphical approach. We focused the clinical evaluation of our

approach on paragangliomas (PLGs) since these tumors often exihibit high ^{18}F-FDG uptake values and low proliferation indices. Indeed, we hypothesised that these discrepancies are related to high proportions of unmetabolised ^{18}F-FDG (e.g., unphosphorylated ^{18}F-FDG) that are present in PGL tissue.

Materials and methods

Patients

Six patients with newly diagnosed PGLs and 6 control patients with benign or malignant lesions were included. The control group was composed of 3 benign (1 adrenal hematoma, 1 lung infection, and 1 schwannoma) and 3 malignant lesions (2 lung and 1 oesophageal carcinomas). In accordance with the Local Institutional Guidelines, signed written informed consent was obtained from all patients prior to participation.

^{18}F-FDG PET/CT imaging

The patients fasted for a minimum of 6 hours before ^{18}F-FDG injection (4 MBq/kg), and scanning began approximately 60 min later (50 to 71 min). Blood glucose levels were within the normal range in all subjects at the time of the PET acquisitions. Three-dimensional images were acquired using a GE Discovery ST PET/CT hybrid scanner (General Electric Medical Systems). This scanner has an average axial 3D spatial resolution of 5.2 mm at 1 cm and 5.8 mm at 10 cm from the FOV centre and a maximum sensitivity of 9.3 cps/kBq. The axial and transverse FOV of this scanner are 15.7 and 70 cm, respectively.

The CTs were performed first and extended from the skull base to the upper thigh. The parameters for the CT were as follows: 140 kV, 64 mAs, DLP 388 mGy.cm, and a 5-mm section thickness. The section thickness of CT scans matched the PET slice thickness. Immediately after the CT, a PET that covered the identical transverse field of view with an acquisition time of 3 min per table position (3D mode) was obtained.

Our first whole body PET/CT was performed according to the current recommendations for cancer imaging [2] and helped us to precisely define the target hypermetabolic foci that were chosen for the following 4 additional list-mode acquisitions (3 min each every 5 minutes): t_1, t_2, t_3 and t_4.

The PET image datasets were corrected for randoms, scatter, and decay and iteratively reconstructed (OSEM algorithm) using the CT data for attenuation correction. Co-registered images were displayed on a workstation (Xeleris; GE Healthcare) with 3D representation and transaxial, coronal and sagittal slices.

The 2D-ROIs were manually drawn on the 3 consecutives transaxial PET images surrounding the maximum intensity of the whole lesion. Each 2D-ROI covered at least two-thirds of the lesion surface. The same ROIs were used at each study time point (t_1, t_2, t_3, t_4) For each ROI, the maximum activity concentration in [Bq/mL] and the maximum SUV (SUVmax) were measured.

Venous blood sampling was performed at 4 different time intervals: t_1, t_2, t_3, t_4. which provided four measures of activity of ^{18}F-FDG in the blood at time t_j, noted respectively by $C_{P,j}$ for j = 1,2,3,4. The measurements of blood activity were performed using a Cobra Gamma Counter (Cobra II-Auto Gamma, Packard Instrument Co.). The 3-inch crystal configuration of this counter has a high sensitivity for detecting high-energy annihilation photons. Calibration was performed immediately before the sample measurements.

The counting error, which depends on the count rate, is approximately 1% per 10,000 cps counted, the error on the volume measurement (<1%) and the error on the counting efficiency, which should be estimated to be between 1 to 2%, should be added to this the counting error.

Methods

To determine the unmetabolised fraction of ^{18}F-FDG within the lesion, we considered the standard 3-compartment kinetic model [18]. The k_1, k_2 and k_3 transfer rate parameters characterise the transport between 2 extravascular compartments; k_1 measures the facilitated ^{18}F-FDG transport from the blood into the tissue (a precursor compartment) per unit of tissue volume, k_2 measures the tracer transport from the precursor compartment back into the blood, and k_3 characterises the phosphorylation of ^{18}F-FDG to ^{18}F-FDG-6P (a metabolic compartment), which is assumed to be proportional to hexokinase activity. Our model assumes that, after phosphorylation, the radiotracer is irreversibly trapped in the tissue ($k_4 = 0$), which seems to be an appropriate approximation for various cancer models excluding hepatocellular carcinomas [15].

The unmetabolised ^{18}F-FDG (e.g., the unphosphorylated ^{18}F-FDG) includes the ^{18}F-FDG located in the extracellular and the intracellular spaces. If $FDG(t)$ denotes the tissue concentration of ^{18}F-FDG [Bq/mL] in a target tissue, and $C_P(t)$ denotes the concentration of ^{18}F-FDG in the plasma, once the steady-state is achieved, we have the well-known balance equation:

$$FDG(t)=K_i\int_0^t C_P(\tau)d\tau+VC_P(t) \quad \text{(Eq. 1)}$$

$K_i\int_0^t C_P(\tau)d\tau$ and $VC_P(t)$ represent estimations of the metabolised and unmetabolised ^{18}F-FDG components, respectively. The parameter K_i [min^{-1}] is the so-called “net influx rate constant”; it is a composite rate of metabolised ^{18}F-FDG extracted from the plasma and V [w/o unit], which is the vascular volume fraction in the tissue. The parameters K_i and V are expressed in the following way:

$$\mathrm{K_i}=\frac{\mathrm{k_1 k_3}}{\mathrm{k_2+k_3}} \quad \text{(Eq. 2)}$$

and

$$\mathrm{V}=\frac{\mathrm{k_1}}{\mathrm{k_2+k_3}} \quad \text{(Eq. 3)}$$

From equations (Eq. 2) and (Eq. 3) it follows that:

$$k_3 = \frac{K_i}{V} \quad \text{(Eq. 4)}$$

The primary objective was to determine. K_i and V to obtain estimations of both the metabolised and unmetabolised ^{18}F-FDG components. These parameters depend on k_1, k_2 and k_3 but we do not need to calculate k_1, k_2, k_3 to estimate K_i and V. To identify these parameters with a method that would be feasible in clinical practice, we used a method that is an intermediate between SKA and Patlak graphical analyses. This method is based on a mathematical approach integrates a model of the measurement errors and considers the arterial input function model $C_P(t)$ as proposed by the SKA method of Hunter et al [11].

In the SKA method, $C_P(t)$ is modelled using a tri-exponential function as follows:

$$C_p(t) = A_1 \exp(-b_1 t) + A_2 \exp(-b_2 t) + A_3 \exp(-b_3 t) \quad \text{(Eq. 5)}$$

where b_1, b_2 and b_3 are assumed to be equivalent for all patients and are determined from a set of patients for whom repeated blood sampling has been performed. For each individual patient, A_1 and A_2 are computed from the patient's lean body mass and injected activity. A_3 is obtained by fitting the $C_P(t)$ model to a late blood sample. Eq. 5 is then used to compute the area under the FDG(t).curve up to time t:

$$AUC(t) = \int_0^t C_P(\tau) d\tau \quad \text{(Eq. 6)}$$

The K_H index estimates the K_i index based on the SKA method and is obtained by dividing the tumour *FDG* uptake by the AUC under the assumption that the distribution volume of ^{18}F-FDG (V in Eq. 1) can be neglected.

$$K_H = \frac{FDG(t_1)}{AUC(t_1)} \quad \text{(Eq. 7)}$$

In our study, K_H was calculated using the b_1, b_2, and b_3 parameters provided in the work published by Hunter et al. [11]. As in the papers of Hunter et al., $A_1 = A_2$ is the ratio of the injected dose to the blood volume, which is approximately equal to 70 mL per kilogram of lean body mass [10]. The constant A_3 was computed for each patient by fitting the $C_P(t)$ model to a late t_1 blood sample.

Because K_i and V are independent of time, PET/CT images and venous blood samples can be performed at 4 different time intervals during the kinetic process. Given that a plateau phase can be observed to have small differences in terms of maximum activity concentrations, our model also accounted for the variability's of the measurements of FDG_j and $C_{p,j}$ as follows:

$$FDG(t_j)=FDG_j+\varepsilon_j \quad \text{(Eq. 8)}$$

$$C_P(t_j)=C_{P,j}+\bar{\varepsilon} \quad \text{(Eq. 9)}$$

where FDG_j is the maximum concentration averaged over the 3 2D-ROIs that were previously defined within the lesion at t_j. The function $C_P(t)$ is given by Hunter's model and assuming that the experimental model error is given by ε and for j = 1,2,3,4 by ε_j. The random variables $\bar{\varepsilon}$ and ε_j were distributed normally with mean 0 and with respective variance σ^2 and σ_j^2 of the measurements at time t_j. The error on the counting efficiency being estimated between 1 to 2% allows to estimate σ^2 and at each acquisition time, 3 values of maximum activity concentration were obtained which enables an estimate of the variance σ_j^2 of $FDG(t_j)$.

For each measurement of FDG_j and $C_{P,j}$ we drew 10000 random samples of the $\bar{\varepsilon}$ and ε_j from a normal distribution with parameters 0 and σ^2 and 0 and σ_j^2, respectively. The number of random samples (n=10000) was selected based on the well-known Berry–Esseen inequality that specifies the rate at which convergence occurs by bounding the maximal error between the normal distribution and the true distribution of the scaled sample mean. With a convergence rate of $n^{-\frac{1}{2}}$, for n = 10000 the error is less than 10^{-2}. Next, given that $K_i \leq K_H$ because the calculation of K_H neglects the unmetabolised ^{18}F-FDG, we obtained the values of K_i and V by minimising the following functional:

$$f(x,y)=\sum_{j=1}^{4}\left(x\int_0^{t_j}C_P(\tau)d\tau+yC_P(t_j)-(FDG_j+\varepsilon_j)\right)^2 \quad \text{(Eq. 10)}$$

for $0 \leq x \leq K_H$ and $0 \leq y$.

That is, we obtain K_i and V as follows:

$$[K_i,V]=\underset{x\leq K_h,0\leq y}{\operatorname{argmin}} f(x,y) \quad \text{(Eq. 11)}$$

Then, for each value FDG_j and $C_{p,j}$ obtained by Eq. 8 and Eq. 9, and after using the method of least-squares which consists in minimizing the functional shown in Eq. 10 (minimization was performed using the classic Quasi-Newton method, which implemented in the software Matlab we obtained 10000 values for K_i and V and then deduced their mean values.

Using the mean values previously obtained for K_i and V, the estimations of the percentages of both the metabolised and unmetabolised ^{18}F-FDG components at t were simple and are denoted by pM(t) and pUM(t) respectively:

$$pM(t)=\frac{K_i\int_0^t C_P(\tau)d\tau}{K_i\int_0^t C_P(\tau)d\tau+VC_P(t)} \quad \text{(Eq. 12)}$$

$$pUM(t)=\frac{VC_P(t)}{K_i\int_0^t C_P(\tau)d\tau+VC_P(t)} \quad \text{(Eq. 13)}$$

It follows that, for any time *T*, the mean values of *pM and pUM* between 0 and *T*, which we were called μ*pM*(*T*) et μ*pUM*(*T*) are given respectively by:

$$\mu pM(T)=\frac{1}{T}\int_0^T pM(t)dt \quad \text{(Eq. 14)}$$

$$\mu pUM(T)=\frac{1}{T}\int_0^T pUM(t)dt \quad \text{(Eq. 15)}$$

In the following μ*pUM*(60) will be noted *PUM*; therefore, *PUM* is the mean percentage of unmetabolized 18F-FDG between 0 and *T* = 60 *mn*. (Table 2).

We were also able to calculate the time required to reach 80% of the amount of metabolised ^{18}F-FDG (T80%). Note that T80% characterises the rate of metabolism and is obtained as the single solution of the following equation:

$$pM(t)=0.8 \quad \text{(Eq. 16)}$$

The above equation (Eq. 16) can be easily solved numerically, and a T80% value can be estimated for each patient.

PGL confirmation

We focused the clinical evaluation of our approach on paragangliomas, which exhibit discrepancies between their low proliferation indices and high SUVs that are potentially explained by the contribution of unmetabolised 18F-FDG to the SUV values.

Histopathological analyses of the PGLs were considered the gold standard for the final diagnoses of PHEO/PGL and was obtained in 5 cases (cases 7–11). In the latter case, the diagnosis of PGL was made by a second imaging procedure using 3,4-dihydroxy-6-[(18)F]-fluoro-L-phenylalanine (18F-DOPA) which is considered as a specific tracer for head and neck PGL (HNPGL). ^{18}F-FDOPA, and ^{123}I -MIBG imaging were performed in HNPGLs and PHEOs respectively. For ^{18}F-FDOPA, patients fasted for 3 hours before ^{18}F-FDOPA injection (IASOdopa®, 4 MBq/kg). ^{18}F-FDOPA PET/CT was performed without carbidopa pre-treatment. The PET emission scan started approximately 60 minutes after ^{18}F-FDOPA injection. Three-dimensional images were acquired using a GE Discovery ST PET/computed tomography (CT) hybrid scanner (General Electrics Medical System). For ^{123}I – MIBG scan, patients received at least 200 MBq intravenously (mean 220 MBq) and were evaluated at 24h post-inejection by planar whole-body scan (8 cm/min) using a dual head camera (ECAM, Siemens).

Statistics

All statistical tests were two-sided, non-parametric and performed using SPS 17.0 (SPSS Inc., Chicago, IL, USA). P-values less than 0.05 were considered statistically significant. The agreement between K_i and K_H was evaluated using the intraclass correlation coefficient. Mann-Whitney tests were used for pairwise comparisons of the continuous measures between groups. Spearman's rank correlation coefficients were calculated to assess the associations of the measures and kinetic parameters with the unmetabolised and metabolised ^{18}F-FDG compartment.

Results

Table 1 shows the results of the evaluation of the robustness of the methodology. In the first part of table 1, we performed a test-retest evaluation that involved repeating the calculations for each lesion 5 times. As shown in the table, the repeatability was very good with coefficients of variation below 2% regardless of the kinetic parameters considered.

Next, we assessed the robustness of our method across the time points t_1, t_2, t_3, t_4. For each patient, we computed the same parameters while considering the six 2 time points:

$$(t_1,t_2),(t_1,t_3),..,(t_3,t_4)$$

and the four 3 time points:

$$(t_1,t_2,t_3),(t_1,t_2,t_4),(t_1,t_3,t_4),(t_2,t_3,t_4).$$

Note that for each time points of the calculation for K_H becomes:

$$K_H=\frac{FDG(t_{first})}{AUC(t_{first})}$$

where $t_{first} = t_1$, t_2 *or* t_3 is the first measurement time considered as the case.

Then, the function to minimize becomes

$$f(x,y)=\sum_{j\in J}\left(x\int_0^{t_j}C_P(\tau)d\tau+yC_P(t_j)-(FDG_j+\varepsilon_j)\right)^2$$

where the set J is for 2 or 3 time points respectively :

$$J=\{t_1,t_2\},\{t_1,t_3\},..,\{t_3,t_4\}\text{or}J=\{t_1,t_2,t_3\},..,\{t_2,t_3,t_4\}.$$

As shown in the second part of table 1, the parameters were close to those obtained with all 4 time points. The maximum error for k_3 with respect to 4 time points was less than, 16% and 7.5%, for 2 and 3 time points respectively.

The results of the examination of the clinical feasibility of our method are given in table 2, which shows the kinetic parameter estimates for all patients. Example images are shown in Figures 1 and 2. The agreement between K_i *and V* as excellent (intraclass correlation coefficient=0.996, 95% confidence interval [0.982 to 0.999]).

This group of tumours was composed of 2 adrenal PGLs and 4 head and neck PGLs (HNPGLs). At the time of the study, all of the PGLs were considered as sporadic (based on the absence of a germline mutation in one of the susceptibility genes) and benign because malignancy is defined by the presence of metastatic lesions in which chromaffin cells are not typically present (i.e., lymph nodes, liver, lung, and bones). The Ki-67 proliferative indices were <1% in all operated cases. The PGLs were characterised by high dispersions of the *SUVmax* (9.7 ± 11, coefficient of variation CV=114%), K_i (0.0137 ± 0.0119, CV=87%), and *V* (0.292 ± 0.306, CV=105%) values and lower dispersions of the values of the new parameters k_3 (0.050 ± 0.007 min^{-1}, CV=14%), PUM (33.0 ± 3.9, CV=12%) and T80% (38.34 ± 6.64, CV=17%).

The malignant lesions were characterised by higher values of SUVmax, k_3 and metabolised ^{18}F-FDG fraction compared to the control lesions ($p < 0.05$).

The SUVmax values were not significantly different between the PGLs and the malignant lesions (p=0.44). The unmetabolised ^{18}F-FDG fraction was found to be an important component of the ^{18}F-FDG activities in the defined regions of all of the PGLs (median: 32.0%) and was higher in these lesions than in the malignant lesions (median: 24.0%). In the PGLs, high PUM values were significantly associated with low k_3 ($\rho = -0.99$, $p < 0.001$) values. The PGLs were associated with higher T80% (p=0.02) values and lower k_3 (p=0.02) values relative to the malignant lesions. Lastly, the PUM, k_3 and T80% values of the PGLs were similar to those of the benign lesions (p=0.20).

Discussion

Standardised uptake value (SUV) is hampered by many simplifications and approximations, and the calculations of more reliable quantitative parameters would be of particular value to *in vivo* assessments of tumours at the molecular level [4, 5]. In the present study, we proposed a new methodology to calculate the metabolised and unmetabolised ^{18}F-FDG fractions. We have evaluated this approach on PGLs because these lesions exihibit low proliferation indices and high uptake values, a finding that could be potentially attributable to the contribution of unmetabolised ^{18}F-FDG to the SUV values.

In recent years, the use of PET/CT in PGL imaging has been increasing rapidly [20, 23]. These tumours, especially those associated with succinate dehydrogenase (SDH) mutations, are associated with high positivity on ^{18}F-FDG PET [1, 20–23, 25]. These tumours often exhibit high SUVs despite their high degree of histological differentiation and low proliferation indices. Hypothetically, the activation of hypoxia signalling pathway has been invoked to explain the discordance between high ^{18}F-FDG uptake and low proliferation (pseudo-hypoxia model) [26].

The present results suggest that PGLs are characterised by a relatively low ^{18}F-FDG metabolic activity as expressed by the k_3, *PUM* and T80% values; contrasting with the high SUVmax values. Interestingly, PGLs with highly elevated *SUVmax* values were associated with higher K_i and V values but relatively low k_3 values. From the pathophysiological standpoint, these findings might be related to the high uptake of ^{18}F-FDG (via increased expression or activity of transporters) and a relatively low level of glycolytic activity. It is also notable that these new parameters exhibited lower CV values and should thus be more reliable than *SUVmax* and K_i.

Despite the growing clinical relevance of ^{18}F-FDG PET in oncology, little is known about the molecular determinants of tracer uptake in different types of tumours. Enhanced uptake and metabolism of glucose are frequently observed characteristics of most cancer cells and are associated with alterations to intrinsic energy metabolism that involve a shift from oxidative phosphorylation (OXPHOS) to aerobic glycolysis; this shift is referred to as the Warburg effect. The molecular mechanisms that underpin the metabolic reprogramming of cancer cells are complex and can involve adaptive responses to the tumour microenvironment such as hypoxia or mutations in enzymes or oncogenes that control cell metabolism [24].

PGLs associated with SDH or VHL genes mutations exihibit high positivity on ^{18}F-FDG PET [1, 20–23, 25].

These results suggest that inactivation of the VHL and SDHx genes can upregulate specific HIF downstream targets (pseudohypoxia) and promote tumour growth, angiogenesis, and glycolysis. However, our results suggest that the high proportion of unmetabolised ^{18}F-FDG fraction in PGLs might be related to a lower rates of glycolysis than previously expected and to low proliferation rates. This supposition is consistent with the low k_3 (i.e., the rate of ^{18}F-FDG phosphorylation) values observed in our PGLs, which are known to depend on hexokinase activity. K_i might be elevated in some cases but is more likely to indicate ^{18}F-FDG uptake via GLUT overexpression.

These results are consistent with experimental studies that have also failed to identify overexpression of HIF-1α and genes involved in glycolysis in most tumours [3, 7, 14, 17].

The high SUVs observed in PGLs are also currently not well explained or reflected by histopathological findings (differentiation, proliferation). These findings are also consistent with our preliminary results showing very low tumour ^{18}F-FLT (fluoro-L-thymidine) uptake values despite very high ^{18}F-FDG uptakes (manuscript submitted).

The unmetabolised ^{18}F-FDG includes the ^{18}F-FDG located in various compartments, including the extracellular spaces (in the blood and in the intercellular spaces) and in the cells (e.g., neuroendocrine cells and endothelial cells). In the present study, the PGLs were found to exhibit higher *PUM* and T80% values than the malignant lesions. It is possible that PUM might be influenced by genotype, but our cases had no mutations in one of the SDH genes.

We acknowledge several limitations to our study, including the small sample size, the absence of respiratory gating for 3-dimensional PET of the thorax, and the lack of partial volume effect correction (lesion maximum diameter from 15 to 60 mm).

We assessed the robustness of this approach that was initially designed to consider 4 time points by using 3 or even 2 time points. Encouraging results were obtained (cf. Table 1). Another limitation of this study was the choice of 3 different 2D-ROIs surrounding the entire lesion to obtain the lesion maximum concentrations to derive the clinical variability of the FDG measurements, which yielded single K_i, *V and* k_3 values for the entire lesion. This solution maximised the FDG measurement variability and thus might have increased the errors in the K_i and V estimates. Further improvements are being developed to overcome these limitations. Our method was designed to be easily used in clinical routine (computation time below one minute per lesion). Other potential improvements might include the obtention of the plasma time-activity curve from left-ventricle PET images [13] and a pixel-based generalisation of the methodology.

Another way of methodology improvement would be the use of regularized image reconstruction algorithm, recently implemented on the GE PETscans. Using this new algorithm, the image noise would be largely reduced and the K_i and V estimation largely improved.

This study should be considered as a pilot case study and needs to be further evaluated in a larger study including more tumors with different genetic backgrounds.

Conclusion

In conclusion, the determination of the unmetabolised component can be of particular value to *in vivo* assessments of tumours at the molecular level. In this study, we proposed a new methodology for determining the metabolised and unmetabolised fractions of ^{18}F-FDG. If our findings are prospectively confirmed in a larger patient population, they might provide a new approach for tumor characterisation by imaging and kinetic parameters should be evaluated as predictive biomarkers of malignancy.

Acknowledgements

This study was partly supported by a grant from Rotary Club of the Tholonet, in Aix-En-Provence. We wish to thank the patients who agreed to participate in the present study. The authors also wish to thank the technologists in the Department of Nuclear Medicine for their help in the management of the patients for this study. We lastly gratefully acknowledge Dr. I. Buvat for their help in improving this manuscript.

References

1. Blanchet EM, Gabriel S, Martucci V, Fakhry N, Chen CC, Deveze A, Millo C, Barlier A, Pertuit M, Loundou A, et al. (18) F-FDG PET/CT as a predictor of hereditary head and neck paragangliomas. European journal of clinical investigation. 2014; 44:325–332. [PubMed: 24422786]
2. Boellaard R, O'Doherty MJ, Weber WA, Mottaghy FM, Lonsdale MN, Stroobants SG, Oyen WJ, Kotzerke J, Hoekstra OS, Pruim J, et al. FDG PET and PET/CT: EANM procedure guidelines for tumour PET imaging: version 1.0. Eur J Nucl Med Mol Imaging. 2010; 37:181–200. [PubMed: 19915839]

3. Burnichon N, Vescovo L, Amar L, Libe R, de Reynies A, Venisse A, Jouanno E, Laurendeau I, Parfait B, Bertherat J, et al. Integrative genomic analysis reveals somatic mutations in pheochromocytoma and paraganglioma. Hum Mol Genet. 2011; 20:3974–3985. [PubMed: 21784903]

4. Cheebsumon P, van Velden FH, Yaqub M, Hoekstra CJ, Velasquez LM, Hayes W, Hoekstra OS, Lammertsma AA, Boellaard R. Measurement of metabolic tumor volume: static versus dynamic FDG scans. EJNMMI Res. 2011; 1:35. [PubMed: 22214394]

5. Cheebsumon P, Velasquez LM, Hoekstra CJ, Hayes W, Kloet RW, Hoetjes NJ, Smit EF, Hoekstra OS, Lammertsma AA, Boellaard R. Measuring response to therapy using FDG PET: semi-quantitative and full kinetic analysis. Eur J Nucl Med Mol Imaging. 2011; 38:832–842. [PubMed: 21210109]

6. Dimitrakopoulou-Strauss A, Strauss LG, Schwarzbach M, Burger C, Heichel T, Willeke F, Mechtersheimer G, Lehnert T. Dynamic PET 18F-FDG studies in patients with primary and recurrent soft-tissue sarcomas: impact on diagnosis and correlation with grading. Journal of nuclear medicine : official publication, Society of Nuclear Medicine. 2001; 42:713–720.

7. Favier J, Briere JJ, Burnichon N, Riviere J, Vescovo L, Benit P, Giscos-Douriez I, De Reynies A, Bertherat J, Badoual C, et al. The Warburg effect is genetically determined in inherited pheochromocytomas. PLoS One. 2009; 4:e7094. [PubMed: 19763184]

8. Freedman NM, Sundaram SK, Kurdziel K, Carrasquillo JA, Whatley M, Carson JM, Sellers D, Libutti SK, Yang JC, Bacharach SL. Comparison of SUV and Patlak slope for monitoring of cancer therapy using serial PET scans. Eur J Nucl Med Mol Imaging. 2003; 30:46–53. [PubMed: 12483409]

9. Graham MM, Badawi RD, Wahl RL. Variations in PET/CT methodology for oncologic imaging at U.S. academic medical centers: an imaging response assessment team survey. Journal of nuclear medicine : official publication, Society of Nuclear Medicine. 2011; 52:311–317.

10. Hapdey S, Buvat I, Carson JM, Carrasquillo JA, Whatley M, Bacharach SL. Searching for alternatives to full kinetic analysis in 18F-FDG PET: an extension of the simplified kinetic analysis method. Journal of nuclear medicine : official publication, Society of Nuclear Medicine. 2011; 52:634–641.

11. Hunter GJ, Hamberg LM, Alpert NM, Choi NC, Fischman AJ. Simplified measurement of deoxyglucose utilization rate. Journal of nuclear medicine : official publication, Society of Nuclear Medicine. 1996; 37:950–955.

12. Keyes JW Jr. SUV: standard uptake or silly useless value? Journal of nuclear medicine : official publication, Society of Nuclear Medicine. 1995; 36:1836–1839.

13. Li X, Feng D, Lin KP, Huang SC. Estimation of myocardial glucose utilisation with PET using the left ventricular time-activity curve as a non-invasive input function. Med Biol Eng Comput. 1998; 36:112–117. [PubMed: 9614758]

14. Lopez-Jimenez E, Gomez-Lopez G, Leandro-Garcia LJ, Munoz I, Schiavi F, Montero-Conde C, de Cubas AA, Ramires R, Landa I, Leskela S, et al. Research Resource: Transcriptional Profiling Reveals Different Pseudohypoxic Signatures in SDHB and VHL-Related Pheochromocytomas. Mol Endocrinol. 2010; 24:2382–2391. [PubMed: 20980436]

15. Okazumi S, Isono K, Enomoto K, Kikuchi T, Ozaki M, Yamamoto H, Hayashi H, Asano T, Ryu M. Evaluation of liver tumors using fluorine-18-fluorodeoxyglucose PET: characterization of tumor and assessment of effect of treatment. Journal of nuclear medicine : official publication, Society of Nuclear Medicine. 1992; 33:333–339.

16. Patlak CS, Blasberg RG, Fenstermacher JD. Graphical evaluation of blood-to-brain transfer constants from multiple-time uptake data. J Cereb Blood Flow Metab. 1983; 3:1–7. [PubMed: 6822610]

17. Pollard PJ, El-Bahrawy M, Poulsom R, Elia G, Killick P, Kelly G, Hunt T, Jeffery R, Seedhar P, Barwell J, et al. Expression of HIF-1alpha, HIF-2alpha (EPAS1), and their target genes in paraganglioma and pheochromocytoma with VHL and SDH mutations. J Clin Endocrinol Metab. 2006; 91:4593–4598. [PubMed: 16954163]

18. Romer W, Hanauske AR, Ziegler S, Thodtmann R, Weber W, Fuchs C, Enne W, Herz M, Nerl C, Garbrecht M, et al. Positron emission tomography in non-Hodgkin's lymphoma: assessment of chemotherapy with fluorodeoxyglucose. Blood. 1998; 91:4464–4471. [PubMed: 9616140]

19. Sundaram SK, Freedman NM, Carrasquillo JA, Carson JM, Whatley M, Libutti SK, Sellers D, Bacharach SL. Simplified kinetic analysis of tumor 18F-FDG uptake: a dynamic approach. Journal of nuclear medicine : official publication, Society of Nuclear Medicine. 2004; 45:1328–1333.

20. Taieb D, Sebag F, Barlier A, Tessonnier L, Palazzo FF, Morange I, Niccoli-Sire P, Fakhry N, De Micco C, Cammilleri S, et al. 18F-FDG avidity of pheochromocytomas and paragangliomas: a new molecular imaging signature? Journal of nuclear medicine : official publication, Society of Nuclear Medicine. 2009; 50:711–717.

21. Timmers HJ, Chen CC, Carrasquillo JA, Whatley M, Ling A, Eisenhofer G, King KS, Rao JU, Wesley RA, Adams KT, et al. Staging and functional characterization of pheochromocytoma and paraganglioma by 18F-fluorodeoxyglucose (18F-FDG) positron emission tomography. J Natl Cancer Inst. 2012; 104:700–708. [PubMed: 22517990]

22. Timmers HJ, Chen CC, Carrasquillo JA, Whatley M, Ling A, Havekes B, Eisenhofer G, Martiniova L, Adams KT, Pacak K. Comparison of 18F-Fluoro-L-DOPA, 18F-Fluoro-Deoxyglucose, and 18F-Fluorodopamine PET and 123I-MIBG Scintigraphy in the Localization of Pheochromocytoma and Paraganglioma. Journal of Clinical Endocrinology and Metabolism. 2009; 94:4757–4767. [PubMed: 19864450]

23. Timmers HJ, Kozupa A, Chen CC, Carrasquillo JA, Ling A, Eisenhofer G, Adams KT, Solis D, Lenders JW, Pacak K. Superiority of fluorodeoxyglucose positron emission tomography to other functional imaging techniques in the evaluation of metastatic SDHB-associated pheochromocytoma and paraganglioma. Journal of Clinical Oncology. 2007; 25:2262–2269. [PubMed: 17538171]

24. Vander Heiden MG, Cantley LC, Thompson CB. Understanding the Warburg effect: the metabolic requirements of cell proliferation. Science. 2009; 324:1029–1033. [PubMed: 19460998]

25. Venkatesan AM, Trivedi H, Adams KT, Kebebew E, Pacak K, Hughes MS. Comparison of clinical and imaging features in succinate dehydrogenase-positive versus sporadic paragangliomas. Surgery. 2011; 150:1186–1193. [PubMed: 22136839]

26. Vicha A, Taieb D, Pacak K. Current views on cell metabolism in SDHx-related pheochromocytoma and paraganglioma. Endocr Relat Cancer. 2014; 21:R261–R277. [PubMed: 24500761]

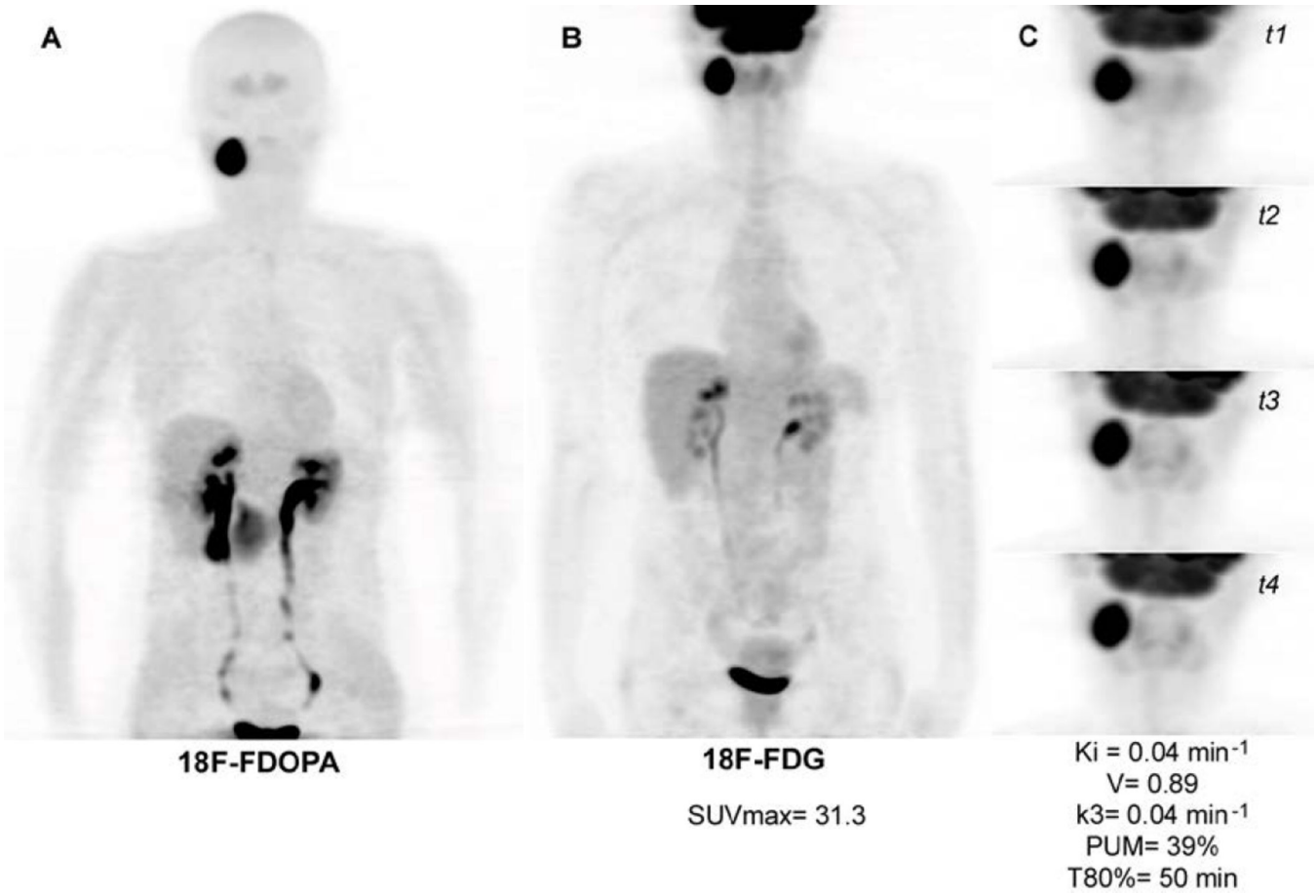

Figure 1.
Cervical PGL. A. ^{18}F-FDOPA PET (maximal intensity projection (MIP)). B. ^{18}F-FDG PET (MIP). C. 4 additional 3D acquisitions centered on the target lesion (^{18}F-FDG PET MIP).

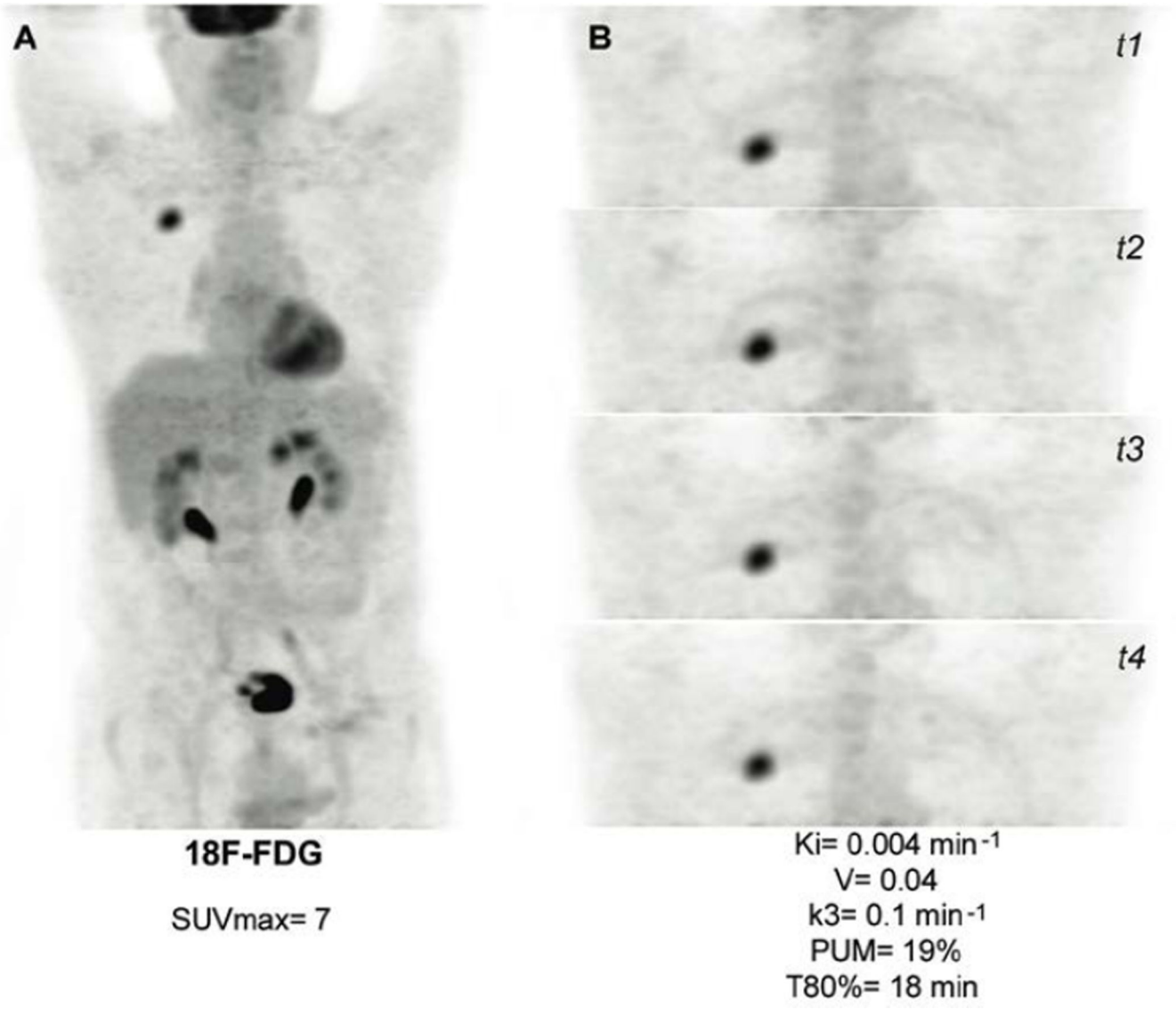

Figure 2.
Lung adenocarcinoma. A. ^{18}F-FDG PET (MIP). B. 4 additional 3D acquisitions centered on the target lesion (^{18}F-FDG PET MIP).

Table 1

Evaluation of the methodology robustness: on the top, a test-retest evaluation, by repeating 5 times the same calculation for one lesion; And on the middle and bottom, the robustness regarding the number of time points t_1, t_2, t_3, t_4 considered (each calculation was repeated 5 times).

test-retest using 4 time points						
	K_H	**Ki**	**V**	**PUM**	**k_3**	**T80%**
	0.0397	0.0362	0.888	0.388	0.041	50.26
	0.0387	0.0358	0.891	0.39	0.04	50
	0.0393	0.0357	0.87	0.386	0.041	49.95
	0.0393	0.0358	0.857	0.383	0.042	49.32
	0.038	0.0356	0.859	0.384	0.041	49.61
mean	**0.039**	**0.036**	**0.873**	**0.386**	**0.041**	**49.828**
std dev	**0.001**	**0.000**	**0.016**	**0.003**	**0.001**	**0.366**
CV	**1.7%**	**0.6%**	**1.8%**	**0.7%**	**1.7%**	**0.7%**
Evaluation using 2 time points						
	K_H	**Ki**	**V**	**PUM**	**k_3**	**T80%**
t1–t2	0.0404	0.036	0.803	0.369	0.045	46.82
t1–t3	0.046	0.0383	0.869	0.373	0.044	47.5
t1–t4	0.0381	0.0345	0.753	0.365	0.046	46.04
t2–t3	0.0387	0.0384	0.867	0.372	0.044	47.29
t2–t4	0.0453	0.0374	0.879	0.379	0.043	48.67
t3–t4	0.0386	0.037	0.587	0.308	0.063	35.71
mean	**0.041**	**0.037**	**0.793**	**0.361**	**0.048**	**45.338**
error vs. 4 time points	**5.6%**	**3.1%**	**9.2%**	**6.5%**	**15.9%**	**9.0%**
CV	**8.6%**	**4.0%**	**14.1%**	**7.3%**	**16.1%**	**10.6%**
Evaluation using 3 time points						
	K_H	**Ki**	**V**	**PUM**	**k_3**	**T80%**
t1–t2–t3	0.0394	0.0355	0.847	0.382	0.042	49.2
t1–t2–t4	0.0375	0.035	0.734	0.358	0.047	44.7
t1–t3–t4	0.0397	0.0371	0.817	0.367	0.045	46.39
t2–t3–t4	0.0386	0.0364	0.862	0.381	0.042	48.99
mean	**0.039**	**0.036**	**0.815**	**0.372**	**0.044**	**47.320**

error vs. 4 time points	0.5%	0.5%	6.6%	3.7%	7.3%	5.0%
CV	2.5%	2.6%	7.0%	3.1%	5.6%	4.6%

Table 2

Summary of parameters derived from the compartment model, performed with the time points t_1, t_2, t_3, t_4.

Patient N°	Final diagnosis	SUVmax	Lesion max diameter mm	K_H min^{-1}	K_i min^{-1}	V	k_3 min^{-1}	PUM (%)	T80 % min
1	Adrenal Hematoma	1.8	45	0.00228	0.00226	0.05	0.045	36.6	46
2	Schwannoma	2.2	40	0.00444	0.0042	0.104	0.04	37	48.5
3	Pneumopathy	6.3	30	0.0144	0.0136	0.29	0.046	33	42
4	Lung Adenocarcinoma	7	15	0.00411	0.00402	0.04	0.099	19	18
5	Lung Adenocarcinoma	10	30	0.0213	0.021	0.224	0.093	25	26.4
6	Esophagus Epidermoid carcinoma	7.5	60	0.013	0.0129	0.154	0.083	24	24.7
7	Adrenal PGL	3.8	24	0.00273	0.00267	0.062	0.043	36	40.4
8	Adrenal PGL	7	25	0.0136	0.0131	0.241	0.054	31	35
9	HNPGL	3.4	51	0.01	0.0095	0.163	0.058	28	30.2
10	HNPGL	31.3	46	0.0387	0.0358	0.891	0.04	39	50
11	HNPGL	10	58	0.0159	0.0157	0.295	0.053	32	37.8
12	HNPGL	2.4	45	0.00538	0.00518	0.101	0.05	32	36.6

Med Biol Eng Comput. Author manuscript; available in PMC 2016 March 06.